

1 Supplyment for

2 **Measurement Report: Seasonal variation and**
3 **anthropogenic influence on cloud condensation nuclei**
4 **(CCN) activity in the South China Sea: Insights from**
5 **shipborne observations during summer and winter of**
6 **2021**

7 Hengjia Ou¹, Mingfu Cai², Yongyun Zhang¹, Xue Ni¹, Baoling Liang³, Qibin Sun^{4,5},
8 Shixin Mai¹, Cuizhi Sun⁶, Shengzhen Zhou¹, Haichao Wang¹, Jiaren Sun², Jun Zhao¹

9 ¹School of Atmospheric Sciences, Guangdong Province Key Laboratory for Climate Change and Natural
10 Disaster Studies, Southern Marine Science and Engineering Guangdong Laboratory (Zhuhai), Sun Yat-
11 sen University, Zhuhai, Guangdong 519082, China

12 ²Guangdong Province Engineering Laboratory for Air Pollution Control, Guangdong Provincial Key
13 Laboratory of Water and Air Pollution Control, South China Institute of Environmental Sciences, MEE,
14 Guangzhou 510655, China

15 ³Guangzhou Sub-branch of Guangdong Ecological and Environmental Monitoring Center, Guangzhou
16 510006, China

17 ⁴Dongguan Meteorological Bureau, Dongguan, Guangdong, 523086, China

18 ⁵Dongguan Engineering Technology Research Center of Urban Eco-Environmental Meteorology,
19 Dongguan, Guangdong, 523086, China

20 ⁶Southern Marine Science and Engineering Guangdong Laboratory (Zhuhai), Zhuhai, Guangdong
21 519082, China

22

23 *Correspondence:* Mingfu Cai (caimingfu@scies.org) and Jun Zhao (zhaojun23@mail.sysu.edu.cn)

24

25 Text S1-S2, Figure S1-S12, and Table S1-S3

26

27 Text S1 Data quality control

28 In order to mitigate the influence of research vessel emissions on the data and obtain authentic
29 atmospheric measurements in the South China Sea, we applied the following data processing
30 procedures.

- 31 1. In the summer cruise, the exhaust emissions from the ship were released at the stern while the
32 observation station was located at the bow. To account for this, and utilizing the accurate
33 relative wind direction information provided by the meteorological station, we adopted
34 method in Huang et al. (2018) to exclude data within the range of 170 to 250 degrees of
35 relative wind direction and with relative wind speeds exceeding 1 m s^{-1} . Additionally, we
36 removed data during abnormal periods (greater than three times the standard deviation) based
37 on the measurements of black carbon (BC) and pollutant NO_x according to Sun et al. (2023).
- 38 2. In the winter expedition, the ship's exhaust emissions were released at the stern while the
39 observation station was located at the bow. However, due to the lack of accurate relative wind
40 direction information, we employed a similar approach as mentioned above (Sun et al., 2023).
41 We removed abnormal data (greater than three times the standard deviation) based on the
42 measurements of pollutant NO_x and BC during periods identified as anomalies.

43

44

45 Text S2 CE selection of the ToF-ACSM

46 The selection of collection efficiency (CE) was based on previous observation conducted in the
47 South China Sea using the ToF-ACSM (Sun et al., 2023). We primarily considered the influence of
48 two factors: aerosol acidity and the impact of nitrate. The calculation was performed using the
49 following formula (Middlebrook et al., 2012):

50 Effect of high ammonium nitrate fraction (ANMF):

$$51 \quad ANMF = \frac{NO_3^- \times \left(\frac{80}{62}\right)}{SO_4^{2-} + NO_3^- + Cl^- + NH_4^+ + Organics} \quad (1)$$

$$52 \quad CE_{est,ANMF} = 0.0833 + 0.9167 \times ANMF \quad (2)$$

$$53 \quad CE_{dry,ANMF} = \max(0.5, CE_{est,ANMF}) \quad (3)$$

54 Effect of acidity:

$$55 \quad \frac{NH_4^+_{measurd}}{NH_4^+_{predicted}} = \frac{NH_4^+ / 18}{2 \times \left(\frac{SO_4^{2-}}{96}\right) + \left(\frac{NO_3^-}{62}\right) + \left(\frac{Cl^-}{35.5}\right)} \quad (4)$$

$$56 \quad CE_{est,acidity} = 1 - 0.73 \times \left(\frac{NH_4^+_{measurd}}{NH_4^+_{predicted}}\right) \quad (5)$$

$$57 \quad CE_{dry,acidity} = \max(0.5, CE_{est,acidic}) \quad (6)$$

58 As shown in Fig. S2, the ANMF is higher in winter compared to summer, although the impacts are
59 not highly pronounced. On the other hand, the effect of aerosol acidity is more significant in
60 summer and relatively lower in winter. Taking into account these factors and referring to Crenn et
61 al. (2015), we employed temporal-varying $CE_{dry,acidic}$ according to eq. (6) in this study, as shown in
62 Fig. S2.

63

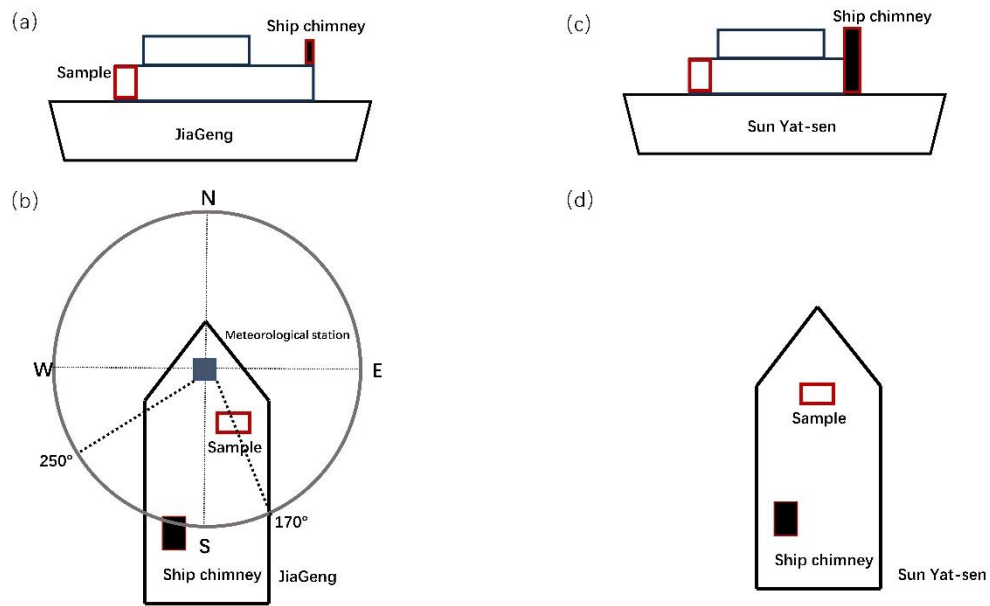
64

65

66

67

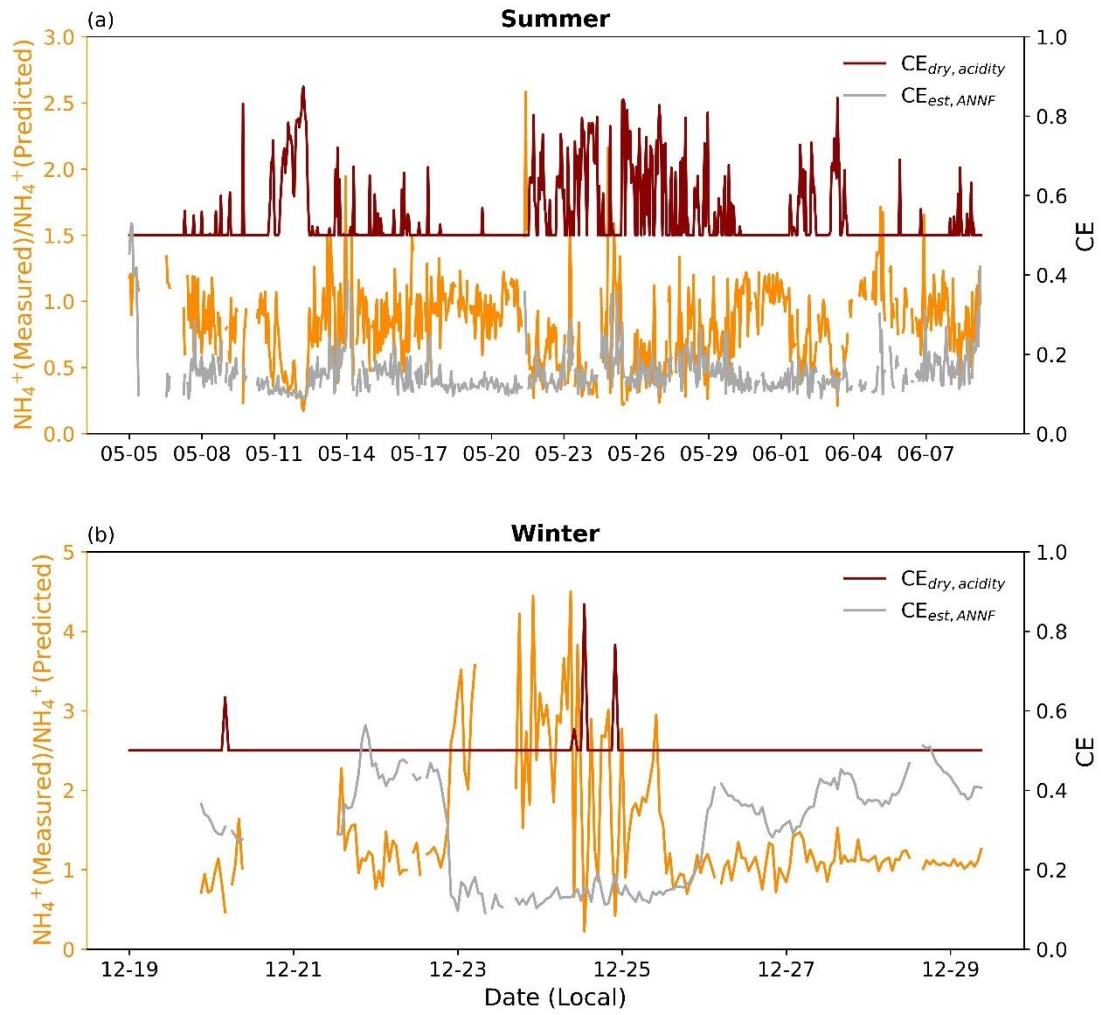
68



69

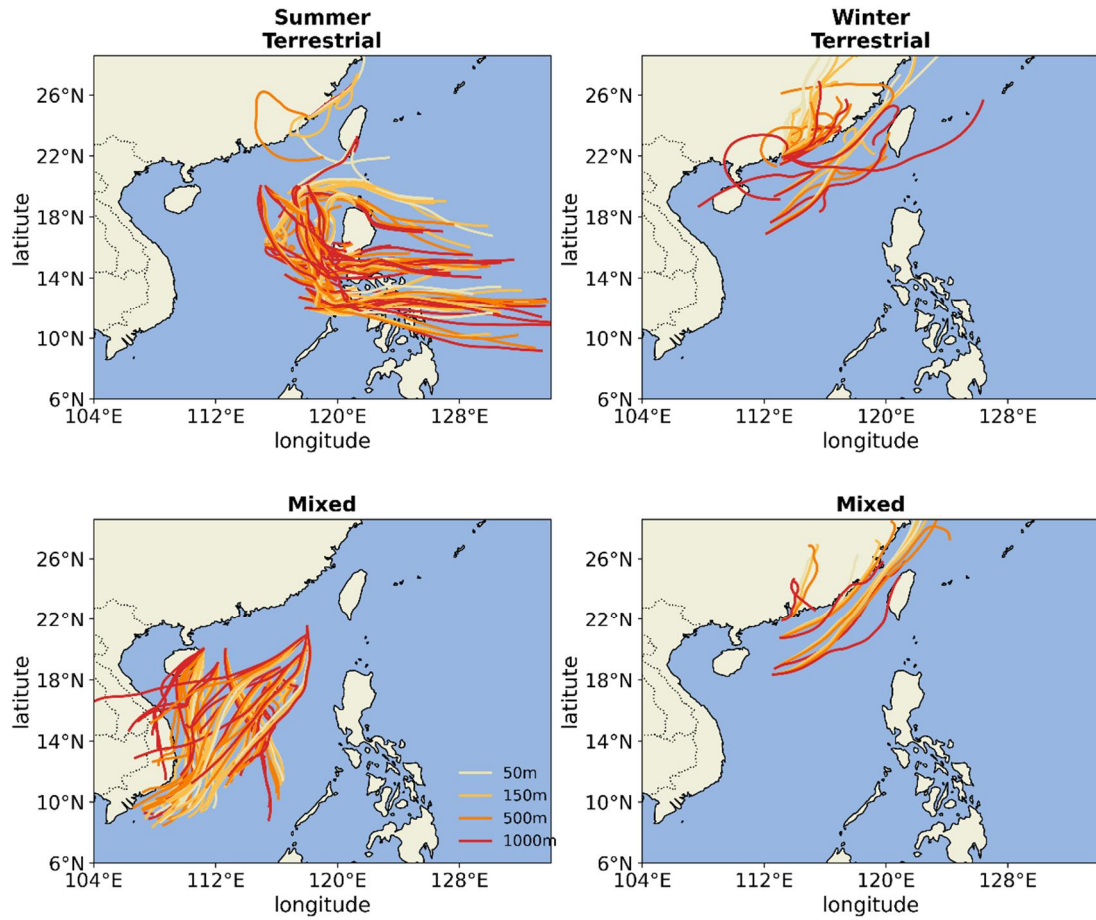
70 **Figure S1. Instrument and ship chimney location in two cruise.**

71



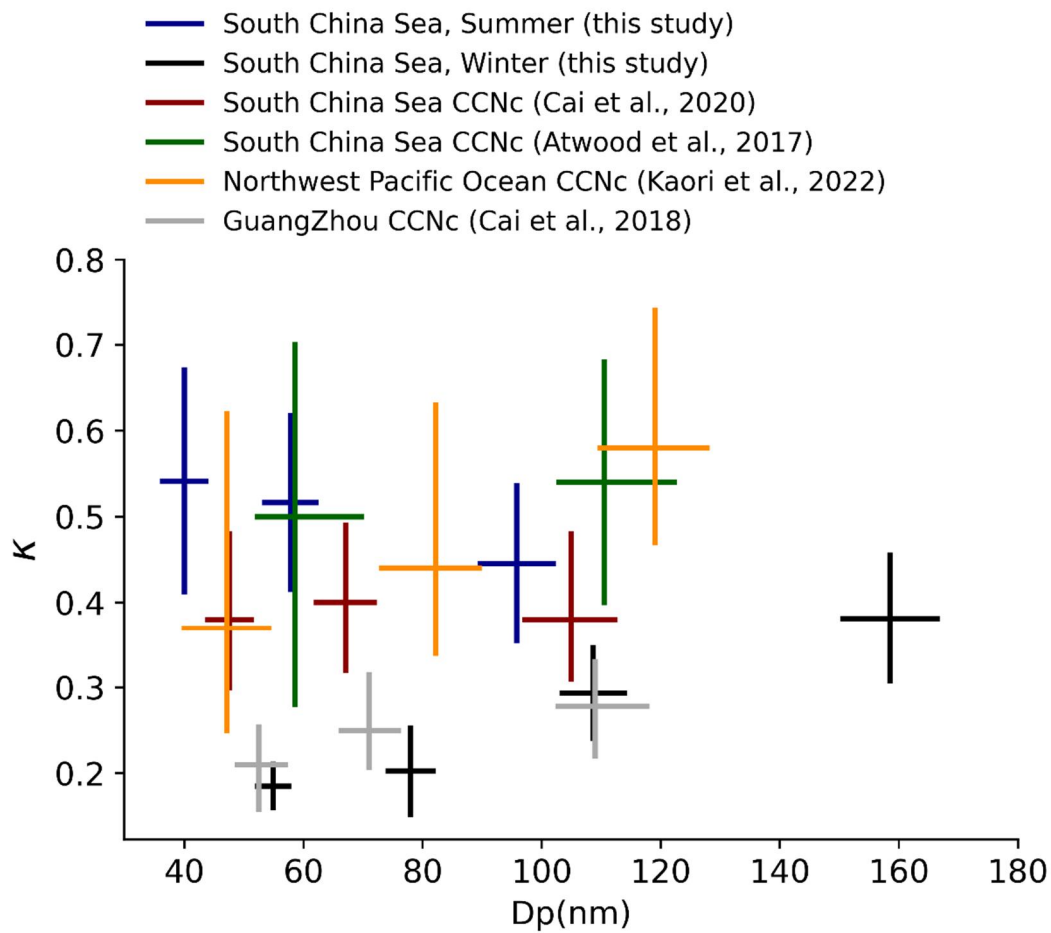
72

73 **Figure S2. Timeseries of $\text{CE}_{\text{dry, acidity}}$, $\text{CE}_{\text{est, ANNF}}$, and $\text{NH}_4^+_{\text{Measured}} / \text{NH}_4^+_{\text{predicted}}$.**



74

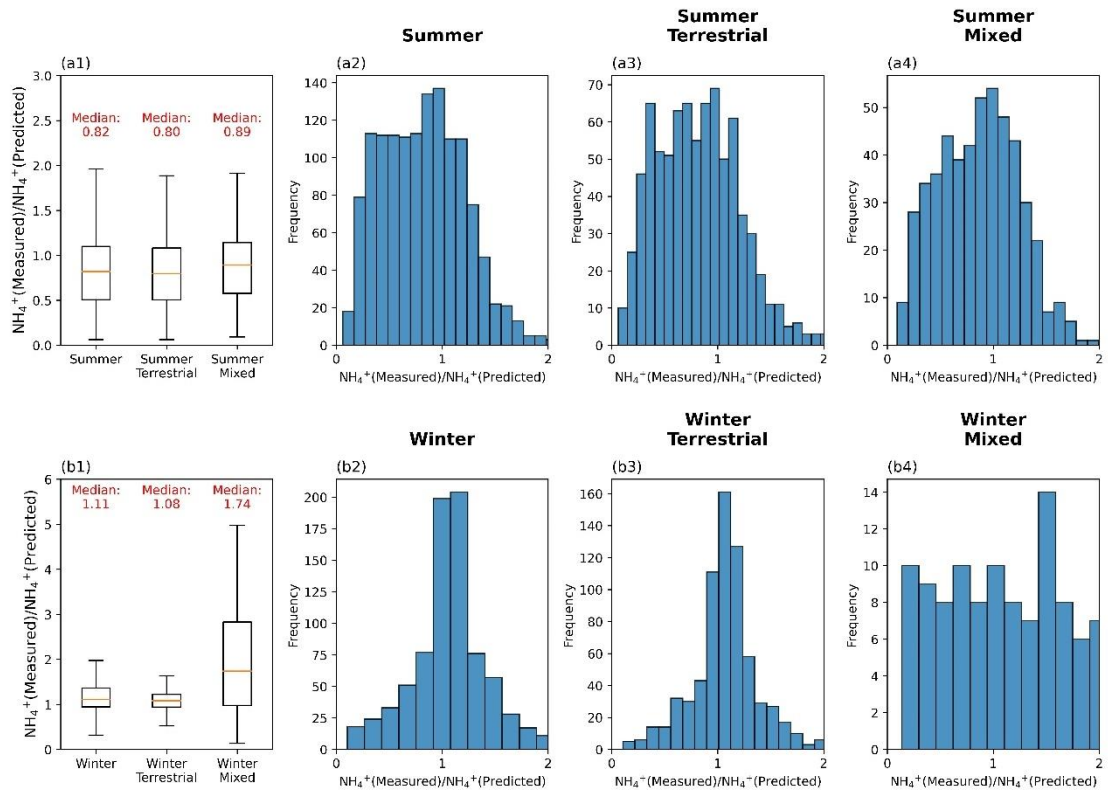
75 **Figure S3. Backward trajectories on 50m, 150m, 500m, and 1000m in summer and winter.**



76

77 **Figure S4. Comparison of activation diameter and κ in this Study with other Studies.**

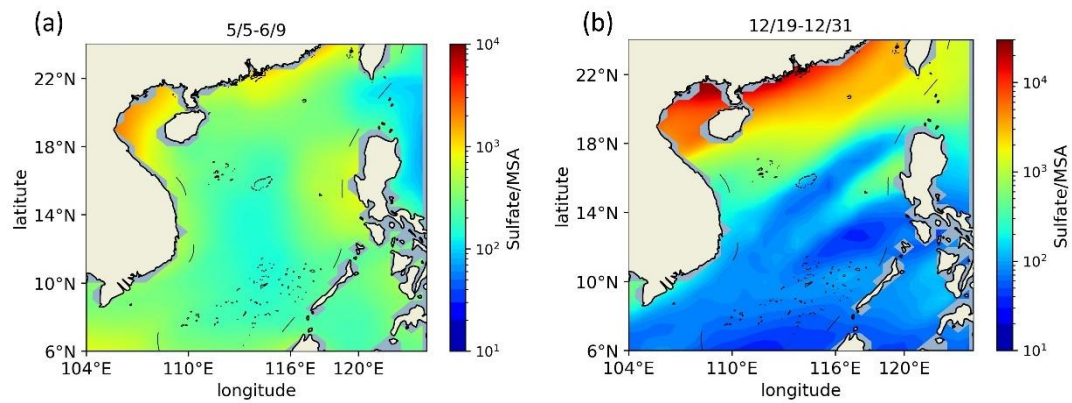
78



79

80 **Figure S5. The value of $\text{NH}_4^+_{\text{Measured}}/\text{NH}_4^+_{\text{Predicted}}$ in all observation and under effect of**
 81 **terrestrial and mixed air masses in summer and winter.**

82

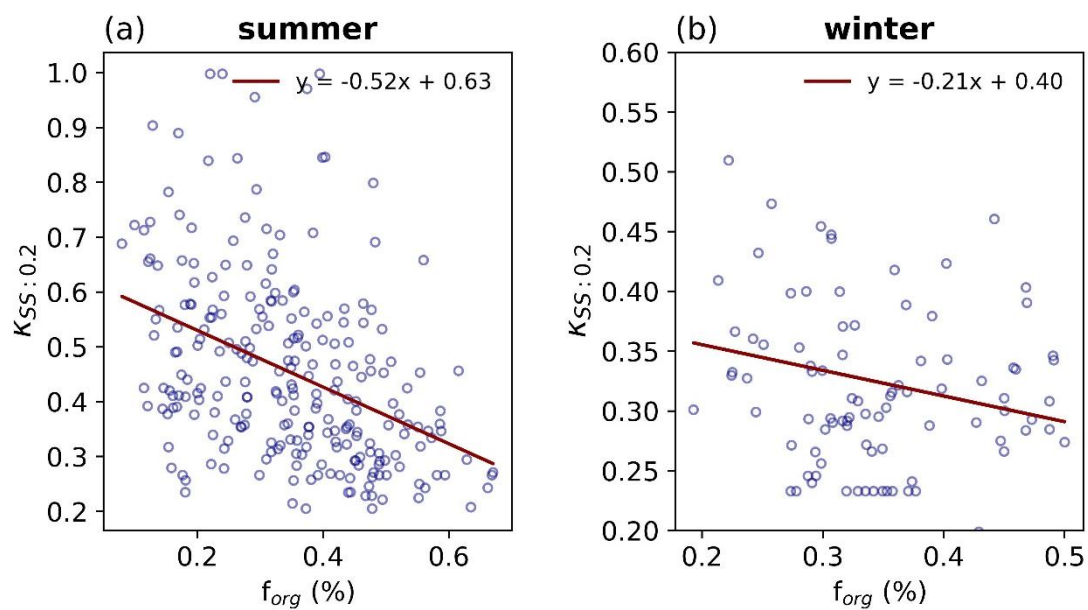


83

84 **Figure S6. The ratio of sulfate to MSA in summer (a) and winter (b).**

85

86

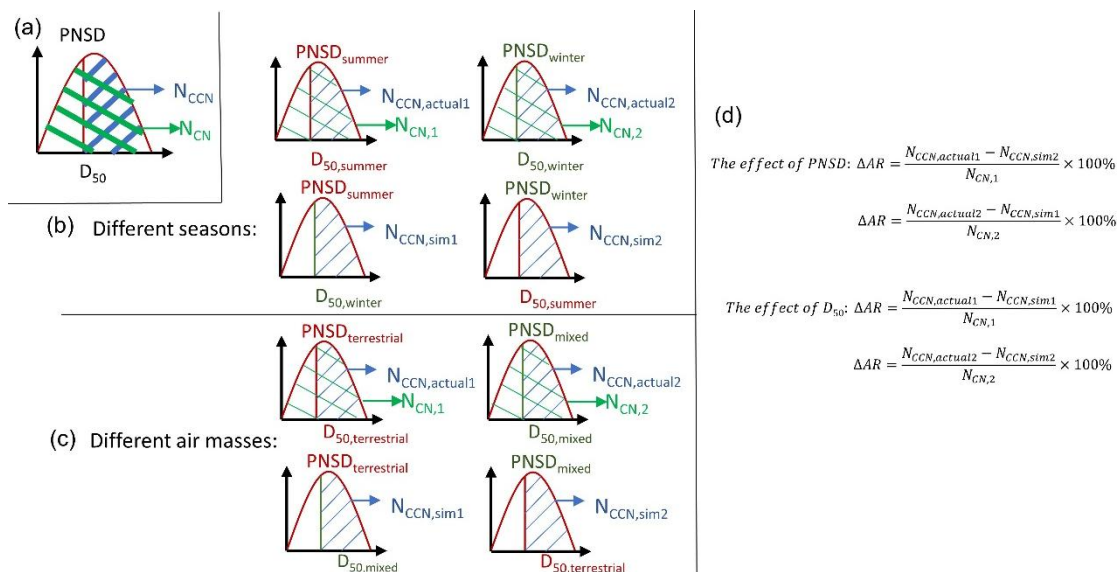


87

88 **Figure S7. Scatter plot of κ under the supersaturation of 0.2% and organic mass fraction**
 89 **with linear regression.**

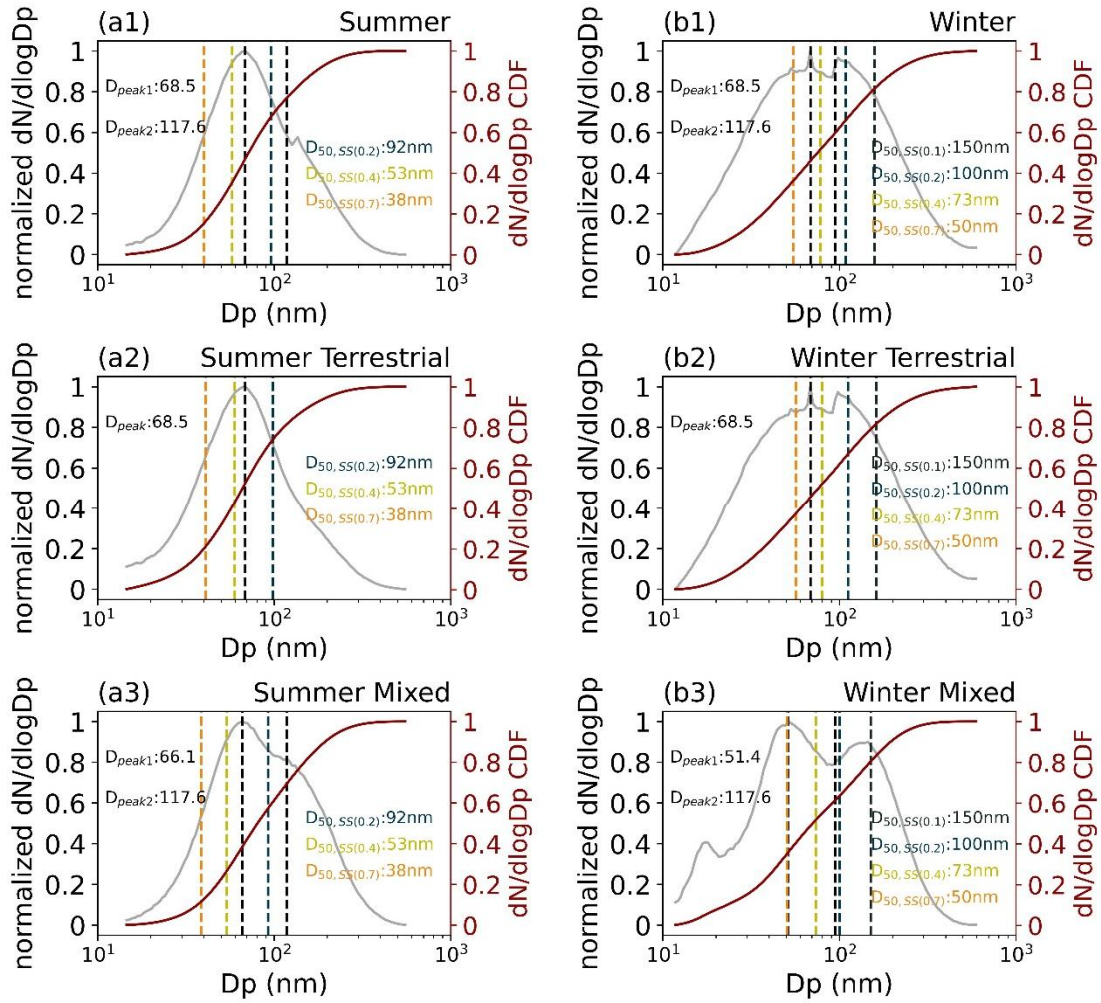
90

91



93

94 **Figure S8. The Calculation Scheme of investigating the effect PNSD and aerosol**
 95 **hygroscopicity (D_{50}) on the activation ratio (AR). (a) The example of total particle and cloud**
 96 **condensation nuclei number concentration calculation; (b) The calculation scheme for**
 97 **different seasons; (c) The calculation scheme for different air masses; (d) the formula of**
 98 **delta AR.**



99

100 **Figure S9. Normalized particle number size distribution and activation diameter at different**

101 **supersaturation under effect of terrestrial and mixed air masses in summer and winter.**

102 **Cumulative distribution function (CDF) is a function that represents the accumulation of**

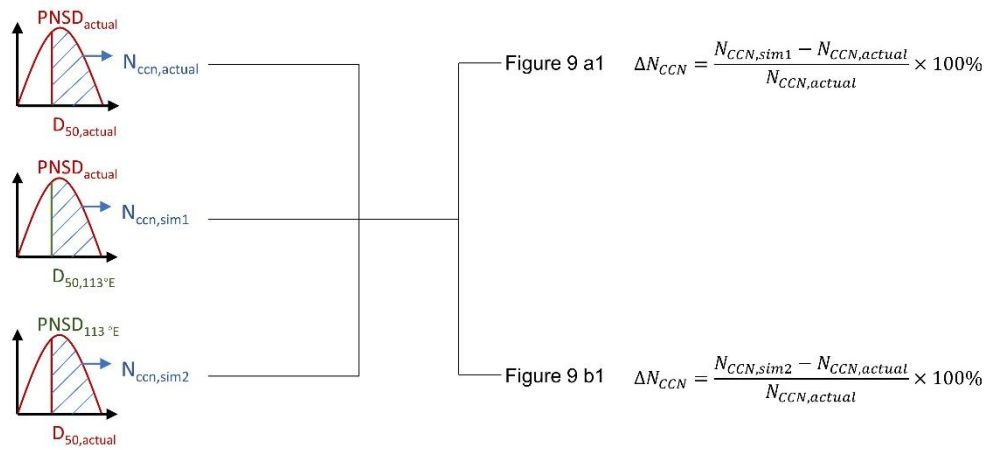
103 **probabilities for values less than or equal to a given value in a statistical dataset.**

104

105

106

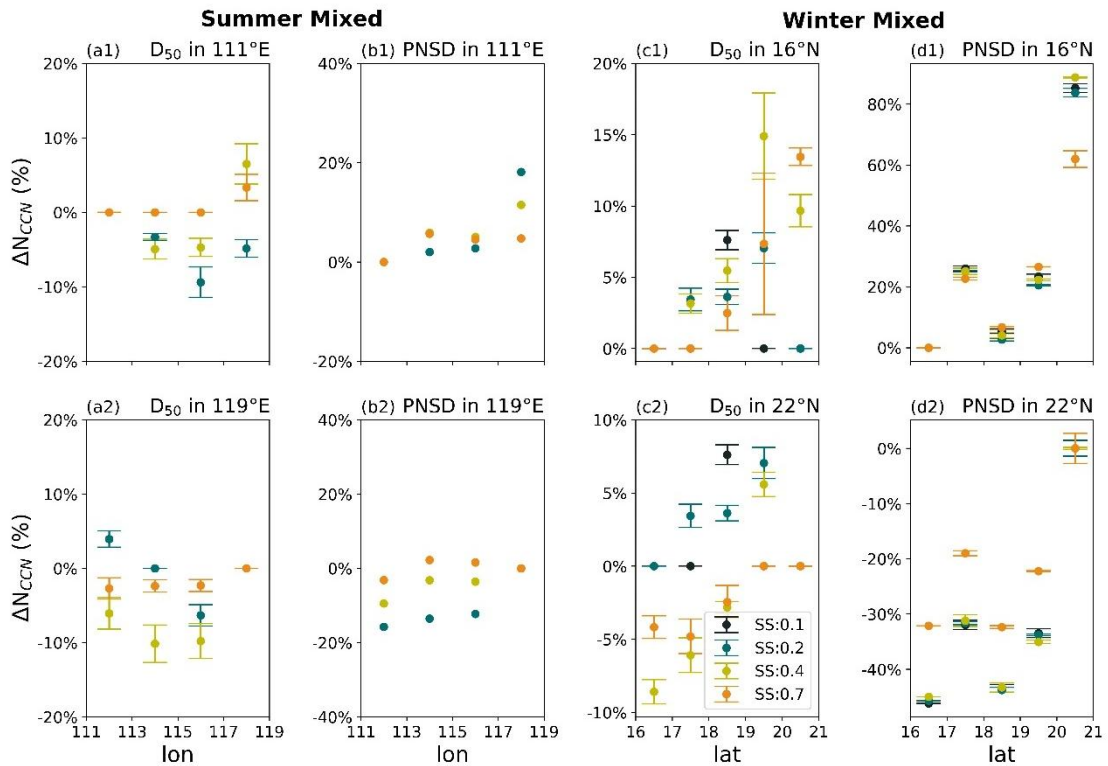
Calculation example of Figure 9



107

108 **Figure S10. The calculation example of Figure 9; the subscript "actual" denotes the**

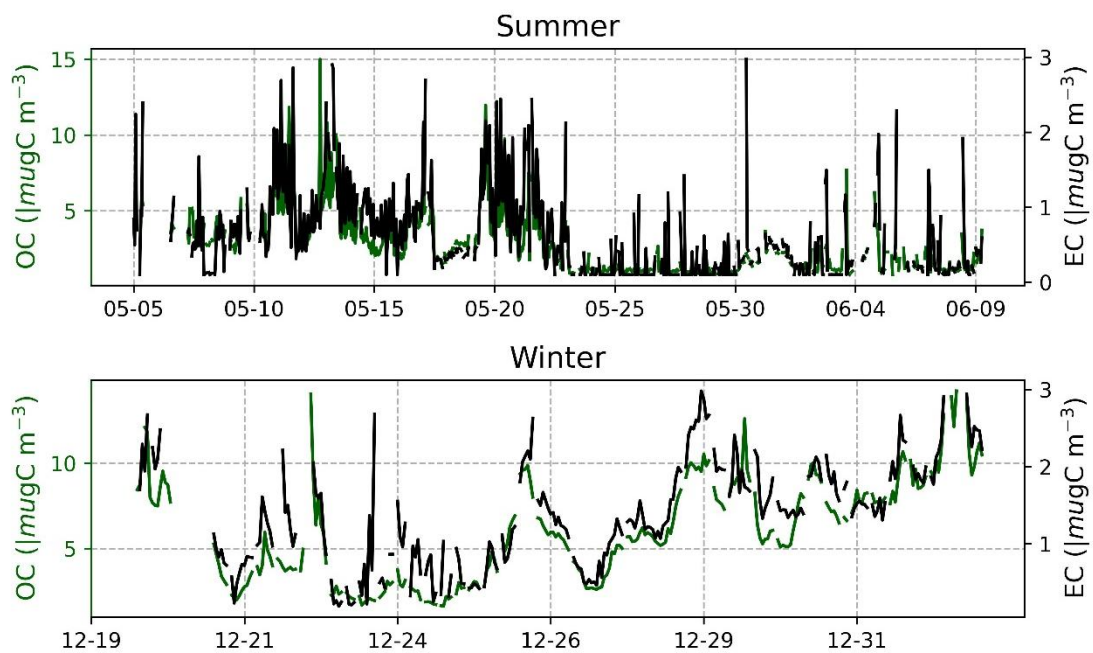
109 **observed values.**



111

112 **Figure S11. The difference between the calculated cloud condensation nuclei (CCN)**
 113 **concentration using the activation diameters from the farthest and nearest offshore**
 114 **distances, along with the measured particle size distribution, and the measured CCN**
 115 **concentration under the effect of mixed air masses in summer (a1 and a2) and winter (c1 and**
 116 **c2); The difference between the calculated CCN concentration using the particle size**
 117 **distribution from the farthest and nearest offshore distances, along with the measured**
 118 **activation diameter, and the measured CCN concentration under the effect of mixed air**
 119 **masses in summer (b1 and b2) and winter (d1 and d2).**

120



121

122 **Figure S12. Timeseries of organic carbon and elemental carbon in summer and winter.**

123

Species	Summer			Winter		
	All	Terrestrial	Mixed	All	Terrestrial	Mixed
Particle number concentration (cm⁻³)						
N _{CN}	7268.85	9921.94	2114.31	4903.73	6336.74	1836.20
PM₁ (µg m⁻³)						
Sulfate	1.44	1.56	1.27	3.47	4.34	1.58
Organic	1.34	1.42	1.22	7.17	9.36	2.42
Nitrate	0.22	0.26	0.17	4.04	5.75	0.29
Ammonium	0.50	0.52	0.47	3.15	3.73	1.91
Chloride	0.08	0.09	0.07	0.28	0.35	0.12
PM_{2.5} (µg m⁻³)						
OC	2.85	3.54	1.54	6.05	6.90	2.45
EC	0.64	0.79	0.36	1.39	1.56	0.65
Gas (ppb)						
SO ₂	1.61	1.74	1.44	2.25	2.43	1.76
NO ₂	9.35	12.82	3.25	47.80	51.06	38.60
NO	32.75	50.73	3.92	9.60	8.66	12.24
CO	279.82	297.54	255.21	69.99	70.02	69.88
O ₃	15.79	15.02	17.07	26.64	20.83	40.17

124 **Table S1. Particle number concentration, mass concentration of NR-PM₁, OC, and EC, gas**
125 **concentration under effect of different air masses in summer and winter.**

126

median diameter (nm)	Summer		Winter	
	Terrestrial	Mixed	Terrestrial	Mixed
All	68.50	66.10	68.5	51.4
Nucleation	19.34±8.01	23.97±7.09	23.95±6.05	20.82±6.76
Aikten	61.40±13.47	60.24±10.50	55.30±18.05	52.51±8.10
Accumulation	151.66±39.75	140.08±27.66	148.59±41.39	144.50±15.98

127 **Table S2. Peak diameter of nucleation, aikten, and accumulation mode under effect of**
128 **different air masses in summer and winter.**

129

Period	ss	0.1%	0.2%	0.4%	0.7%
Summer					
All	$N_{CCN} (cm^{-3})$		2899	5451	5771
	D_{50}		96	58	40
	AR		0.39	0.67	0.85
Terrestrial	$N_{CCN} (cm^{-3})$		3009	6443	7450
	D_{50}		98	60	41
	AR		0.34	0.62	0.81
Mixed	$N_{CCN} (cm^{-3})$		908	1473	1794
	D_{50}		92	54	39
	AR		0.46	0.76	0.89
Winter					
All	$N_{CCN} (cm^{-3})$	881	1661	2357	3053
	D_{50}	156	106	77	54
	AR	0.21	0.36	0.49	0.64
Terrestrial	$N_{CCN} (cm^{-3})$	1049	2209	3341	4445
	D_{50}	158	109	78	56
	AR	0.14	0.29	0.43	0.59
Mixed	$N_{CCN} (cm^{-3})$	752	1189	1524	1909
	D_{50}	150	100	73	50
	AR	0.25	0.40	0.53	0.67

130 **Table S3. Summary of average N_{CCN} , D_{50} , and AR at 0.1, 0.2, 0.4, and 0.7 % ss under effect of**
131 **different air masses in summer and winter.**
132

133 **Reference**

- 134 Crenn, V., Sciare, J., Croteau, P. L., Verlhac, S., Frohlich, R., Belis, C. A., Aas, W., Aijala, M.,
135 Alastuey, A., Artinano, B., Baisnee, D., Bonnaire, N., Bressi, M., Canagaratna, M., Canonaco, F.,
136 Carbone, C., Cavalli, F., Coz, E., Cubison, M. J., Esser-Gietl, J. K., Green, D. C., Gros, V., Heikkinen,
137 L., Herrmann, H., Lunder, C., Minguillon, M. C., Mocnik, G., O'Dowd, C. D., Ovadnevaite, J., Petit,
138 J. E., Petralia, E., Poulain, L., Priestman, M., Riffault, V., Ripoll, A., Sarda-Esteve, R., Slowik, J.
139 G., Setyan, A., Wiedensohler, A., Baltensperger, U., Prevot, A. S. H., Jayne, J. T., and Favez, O.:
140 ACTRIS ACSM intercomparison - Part 1: Reproducibility of concentration and fragment results
141 from 13 individual Quadrupole Aerosol Chemical Speciation Monitors (Q-ACSM) and consistency
142 with co-located instruments, *Atmos Meas Tech*, 8, 5063-5087, doi: 10.5194/amt-8-5063-2015, 2015.
- 143 Huang, S., Wu, Z. J., Poulain, L., van Pinxteren, M., Merkel, M., Assmann, D., Herrmann, H., and
144 Wiedensohler, A.: Source apportionment of the organic aerosol over the Atlantic Ocean from 53
145 degrees N to 53 degrees S: significant contributions from marine emissions and long-range transport,
146 *Atmos. Chem. Phys.*, 18, 18043-18062, doi: 10.5194/acp-18-18043-2018, 2018.
- 147 Middlebrook, A. M., Bahreini, R., Jimenez, J. L., and Canagaratna, M. R.: Evaluation of
148 Composition-Dependent Collection Efficiencies for the Aerodyne Aerosol Mass Spectrometer using
149 Field Data, *Aerosol Sci Tech*, 46, 258-271, doi: 10.1080/02786826.2011.620041, 2012.
- 150 Sun, Q., Liang, B., Cai, M., Zhang, Y., Ou, H., Ni, X., Sun, X., Han, B., Deng, X., Zhou, S., and
151 Zhao, J.: Cruise observation of the marine atmosphere and ship emissions in South China Sea:
152 Aerosol composition, sources, and the aging process, *Environ. Pollut*, 316, 120539, doi:
153 <https://doi.org/10.1016/j.envpol.2022.120539>, 2023.

154